Environmental Science and Pollution Research (2019) 26:31055–31061
https://doi.org/10.1007/s11356-019-06267-8

RESEARCH ARTICLE

Mixed phase nano–CdS supported on activated biomass carbon as efficient visible light–driven photocatalysts

Feng-Ying Cai[1] · Yu-Qing Zhang[1] · Jun-Tao Wang[1] · Jun-Ru Zhou[1] · Hai-Lei Cao[1,2] · Jian Lü[1,3]

Received: 22 April 2019 / Accepted: 16 August 2019 / Published online: 27 August

Abstract

Semiconductors are promising photocatalysts for the use of sunlight in energy conversion and environmental remediation. To this end, various synthetic pathways have been proposed to increase their photocatalytic efficiency, catalytic stability, recycle, and reuse. In this work, mixed phase CdS nanoparticles were loaded on the surface of activated biomass carbons to prepare composite photocatalysts via hydrothermal syntheses, which were further applied to photocatalytic degradation of rhodamine B (RhB) under visible irradiation. The composite photocatalysts displayed considerable specific surface area (up to 672 m^2 g^{-1}) and suitable band gap energy of ca. 2.1 eV. Due to the excellent light adsorption ability and chemical stability, these composite photocatalysts exhibited excellent photocatalytic capacity toward RhB degradation under visible irradiation. Moreover, the photocatalytic stability was also demonstrated by cyclic experiments, by which the composite photocatalysts retained over 80% of the initial catalytic activity after 4 consecutive runs.

Keywords Biomass carbon · Cadmium sulfide · Composites · Photocatalysis

Introduction

The advance of practically applicable photocatalysts for the effective use of solar energy has attracted enormous research attention in environmental remediation (Xiang et al. 2012; Xue et al. 2015; Panneri et al. 2017), in view of the unprecedented demands on sustainable resources and renewable energy supplies (Dai et al. 2012; Poizot and Dolhem 2011; Aricò et al. 2005). In this context, a number of semiconductors have shown great potentials as viable photocatalysts due to their suitable band gap energies, of which the cadmium sulfide (CdS) is particularly efficient in visible light–driven photocatalyses (Ning et al. 2016; Li et al. 2015; Dai et al. 2014; Chen et al. 2010). However, the practical usage of CdS has been largely restricted by serious photocatalytic instability and deactivation related to the photocorrosion (Zhang et al. 2005; Apte et al. 2012; Han et al. 2011). In this circumstance, material supports might become necessary for the separation of photogenerated carriers (electrons and holes) during photocatalysis. Moreover, favorable adsorption and accessibility of organic substrates on surfaces of material supports are achieved, coupled to the possible interplay between substrates and catalytically active sites, which may largely facilitate photocatalytic reactions (Fang et al. 2017).

Biomass carbons (BCs), known also as biochar, are readily fabricated from the pyrolysis of agricultural and garden wastes at high temperature (Singh et al. 2012) and have been developed as one of the key strategies for the sequestration and transportation of carbon, as well as the production of renewable energy (Woolf et al. 2010; Harvey et al. 2012; Rawal et al. 2016). At the same time, BCs are regarded as efficient and eco-friendly remediation materials due to their superior adsorption capacity derived from the high specific surface

Responsible editor: Suresh Pillai

Electronic supplementary material The online version of this article (https://doi.org/10.1007/s11356-019-06267-8) contains supplementary material, which is available to authorized users.

✉ Hai-Lei Cao
caohailei@163.com

[1] Fujian Provincial Key Laboratory of Soil Environmental Health and Regulation, College of Resources and Environment, Fujian Agriculture and Forestry University, Fuzhou 350002, China

[2] Key Laboratory of Functional Inorganic Material Chemistry, Ministry of Education, Heilongjiang University, Harbin 150080, China

[3] Samara Center for Theoretical Materials Science (SCTMS), Samara State Technical University, Samara, Russia 443100

area and porosity, hierarchical porous structures, abundant surface functional groups and mineral compositions (Bunmahotama et al. 2017; Su et al. 2016; Huggins et al. 2016). In the light of the prominent property of BCs, specific research attention has also been focused on the interplay with supported nanoparticles (NPs), further to investigate the synergic effects at interfaces, aiming at functional optimization of NPs. Furthermore, the BCs are intrinsically adaptable to couple with nanoparticles (NPs) of metals and metal oxides/sulfides, by which their capability in contaminant treatment is largely enhanced due to the optimization of pore structure and functionality, as well as the implantation of potential active sites (Liu et al. 2011; Zhao et al. 2008; Jang et al. 2008).

In this work, biomass carbons were used as photocatalyst carriers by means of loading mixed phase CdS semiconductors (mp–CdS) at the surfaces by applying a hydrothermal method to prepare composite materials. The composite photocatalysts were fully characterized and applied for the degradation of rhodamine B (RhB) in aqueous phases. Specifically, the composite photocatalysts inherited high specific surface areas and developed porous structures from activated BCs (1184 $m^2\ g^{-1}$). It was demonstrated that band gaps of the composite photocatalysts (ca. 2.1 eV) were considerably decreased by contrast to the mp–CdS precursor (2.2 eV). The photocatalytic degradation of RhB was evaluated and the mp–CdS@BC–2 exhibited the highest degradation efficiency ($\kappa = 2.7 \times 10^{-2}\ min^{-1}$) which was 3-fold that of the mp–CdS precursor ($\kappa = 9.1 \times 10^{-3}\ min^{-1}$). Moreover, the mp–CdS@BC–2 showed excellent catalytic stability in cyclic experiments, in which more than 80% of the initial photocatalytic activity was remained after four cycles.

Experimental section

Materials

Cadmium acetate dihydrous [$Cd(CH_3COO)_2{\cdot}2H_2O$], thioacetamide, ethanediamine, potassium hydrate (KOH), and RhB were purchased commercially as analytical reagents. Reaction solutions and stock solutions were prepared using deionized water supplied with a UPT–I–5T ultrapure water system.

Preparation of biomass activated carbon

The biomass carbons (BCs) were prepared according to the procedure reported in the literature (Huang et al. 2018). BCs defined pyrolysis and activation via KOH corrosion at 600 °C. Activated BC samples were collected to wash with diluted hydrochloric acid (HCl, 0.1 M) until the filtrates were approximately neutral, which were dried in oven at 70 °C for further use.

Preparation of composites with mixed phase CdS through hydrothermal reactions

Composite-based biomass activated carbon and mixed phase CdS (mp–CdS) were prepared from modified hydrothermal reactions (as shown in Scheme 1). Typically, $Cd(CH_3COO)_2{\cdot}2H_2O$ (533 mg, 2.0 mmol) was added in ethanediamine (60 mL) under magnetic stirring, and thioacetamide (105 mg, 1.4 mmol) was introduced after $Cd(CH_3COO)_2{\cdot}2H_2O$ was completely dissolved and stirred continuously for 1 h. The above solution, after blending with certain amount of as-prepared activated BCs, was transferred and sealed in a solvothermal autoclave and reaction temperature was increased to 180 °C with a heating rate of 1.0 °C min^{-1} and kept in oven for 5 h. After slow cooling to room temperature, the solid sample was washed with ethanol for three times and collected by centrifugation and dried overnight in oven (50 °C). Samples prepared with the addition of 200, 300, and 400 mg BCs were denoted as mp–CdS@BC–1, –2, –3, respectively.

Characterization of mp–CdS@BC composites

Scanning electron microscopy (SEM) images were obtained by using a JSM6700–F working at 10 kV. Transmission electron microscopy (TEM) and high-resolution TEM (HRTEM) images were recorded by using an FEIT 20 working at 200 kV.

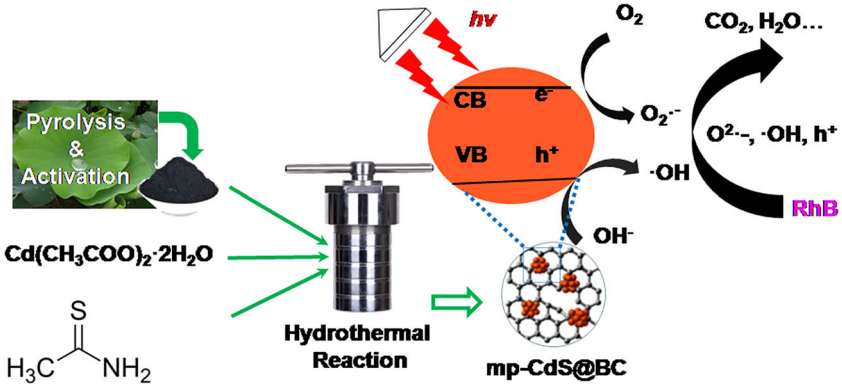

Scheme 1 Schematic reaction pathway of mp–CdS@BC synthesis and photocatalysis

Powder X–ray diffraction (PXRD) were carried out on a Miniflex 600 diffractometer with Cu Ka radiation (λ = 0.154 nm). N_2 adsorption/desorption isotherms and Brunauer–Emmett–Teller (BET) surface area measurements were obtained on a Micromeritics ASAP 2460 instrument. The diffuse reflectance spectra (DRS) were recorded in the range of 200 nm to 800 nm on a Shimadzu UV–2600 UV–vis spectrophotometer with $BaSO_4$ as the background.

Photocatalytic reaction

Photocatalytic reactions were carried out under the illumination of a 300 W Xearc lamp (PLS-SXE300C, Beijing) and 420 and 780 nm cutoff filters were implemented to ensure visible light illumination. The light intensity was tested to be in the range of ca. 2320~2350 Candela. In a typical photocatalytic reaction, 5 mg of composite photocatalyst and 100 mL RhB solution (10 ppm) was added in a Pyrex glass vessel (200 mL) with simultaneous shaking. The above mixture was left for 60 min in dark then exposed to visible light. Photocatalytic experiments were monitored by UV–vis measurements of the characteristic absorbency of RhB after certain time of intervals. Degradation efficiency was estimated by the following equation:

$$D = C/C_0 \times 100\%$$

where D, C_0, and C represented the degradation efficiency, initial, and tested characteristic absorbency of RhB, respectively. Rate constant (κ) was estimated by the following equation:

$$\ln (C_0/C) = \kappa t$$

Photocatalyst stability test

Cycling reactions were performed to test the stability of composite photocatalyst. Between two consecutive runs of a cycling reaction, the photocatalyst was recovered by centrifugation and washed with ethanol for three times until UV absorbance of the filtrates was nearly invisible, and dried at 50 °C in oven. At the end of a cycling reaction, the photocatalyst was separated, washed, and dried as stated above and used for further XRD measurements.

Results and discussion

Characterization of mp–CdS@BC composites

Porosity and surface area

Material porosity is one of the key factors that decide the adsorption affinity and capacity. Therefore, the N_2 adsorption–desorption isotherms of BC and mp–CdS@BC–n (n = 1, 2, and 3) were recorded, which revealed hybrid type I/IV isotherms and showed dominant microporosity (Fig. 1). The specific surface area of BC support was calculated to be ca. 1184 $m^2\ g^{-1}$, whereas those for mp–CdS@BC–n was in the range of 455 and 672 $m^2\ g^{-1}$ (Table 1). The rational decrease in BET of mp–CdS@BC–n was attributable to the loading of CdS nanoparticles (NPs) that partially blocked pores of BC supports. The CdS loading in mp–CdS@BC–n was determined to be 47.3%, 39.9%, and 27.3%, respectively, according to the elemental analyses and ICP measurements (Table 1).

Crystallinity and morphology

Surface morphology of the mp–CdS@BC–2, as a representative material, was investigated by means of the scanning electron microscopy (SEM) and transmission electron microscopy (TEM) techniques. The SEM image exhibited clear domains of mp–CdS being deposited on BC surfaces (Fig. 2a). TEM image identified rod–shaped and cluster nanoparticles, which were assigned to the cubic and hexagonal phases of CdS NPs (Fig. 2b; Fig. S1; ESI). The lattice spacing of rod-like and cluster-like CdS was measured in the HRTEM images (Fig.

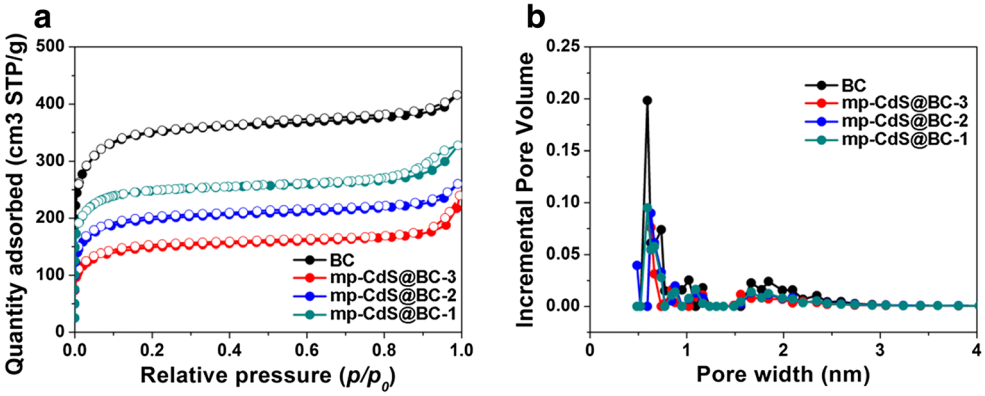

Fig. 1 N_2 adsorption/desorption isotherms (**a**) and pore size distribution (**b**) of BC and mp–CdS@BC–n (n = 1, 2, and 3)

Table 1 Elemental analysis and BET of BC and mp–CdS@BC–n (n = 1, 2, and 3)

Samples	Contents (%)				S_{BET} ($m^2\ g^{-1}$)
	C	H	S	Cd	
mp–CdS@BC–1	27.3	1.6	10.3	36.8	455
mp–CdS@BC–2	34.3	1.7	9.2	31.0	615
mp–CdS@BC–3	42.5	1.9	6.3	21.2	672

2c, d). The lattice spacing of 0.336 and 0.356 nm, correspond to the (1 1 1) lattice plane of cubic CdS and the (1 0 0) lattice plane of hexagonal CdS, respectively. The PXRD patterns of mp–CdS@BC–n were nearly identical to the mp–CdS precursor with diffraction characteristics that were fully indexed to the cubic (JCPDS 10–0454) and hexagonal (JCPDS 41–1049) CdS (Fig. 2e) (Dai et al. 2014; Li et al. 2016). Moreover, the mp–CdS@BC–n showed significantly better crystalline than that of the mp–CdS.

Light adsorption capacity and thermal stability

It was known that mixed phase CdS generally displayed high catalytic efficiency (Dai et al. 2014; Li et al. 2016) and composite photocatalysts could further facilitate the catalytic activity through the introduction of porous material supports. Therefore, UV–vis DRS (Fig. 3a) and TGA (Fig. S2a; ESI) analyses of mp–CdS@BC–n were performed to evaluate their light adsorption capacity and thermal stability related to the possible applicability as viable photocatalysts. In comparison with the mp–CdS, UV–vis DRS of mp–CdS@BC–n exhibited red-shifted absorption bands (Fig. 3a), which indicated improved light harvesting capacity of the mp–CdS@BC–n composite photocatalysts (Matos et al. 2001; Apte et al. 2012). The favorable visible irradiation for mp–CdS@BC–n was also reflected by the band gap narrowing by contrast to that for mp–CdS (ca. 2.1 eV versus ca. 2.2 eV; Fig. 3b). The reduced band gap energy indicated enhanced interactions or the interface contacts between CdS and BC supports (Wu et al. 2017; Jing et al. 2017), and thus strong interfacial interactions or more surface contacts might exist in the mp–CdS@BC–n composite photocatalysts.

Degradation of RhB

Degradation effects

The photocatalytic capacity of mp–CdS and mp–CdS@BC–n nanocomposites were evaluated by RhB degradation in aqueous solutions under visible light irradiation (Fig. 3c). Photocatalysts were first immersed in RhB solutions for 1 h to reach the equilibrium of adsorption/desorption in dark (Fig. S3; ESI), and photocatalytic reactions were carried out thereafter. The mp–CdS@BC–1 (ca. 68.7%) exhibited similar photocatalytic efficiency to the mp–CdS (ca. 65.3%) precursor in 2 h, whereas mp–CdS@BC–2 (> 95.0%) and mp–CdS@BC–3 (ca. 84.2%) showed considerably higher catalytic ability. These results matched well with the UV–vis DRS analyses due to the reduced band gap energy of composite photocatalysts. Meanwhile, the catalytic ability of the composite photocatalysts followed the order of mp–CdS@BC–1 < mp–CdS@BC–3 < mp–CdS@BC–2. Of special notice, the mp–CdS@BC–2, displaying moderate BET surface area and band gap energy, possessed the highest photocatalytic efficiency. Moreover, it was also possible that excessive sulfur elements were doped into the material photocatalysts and

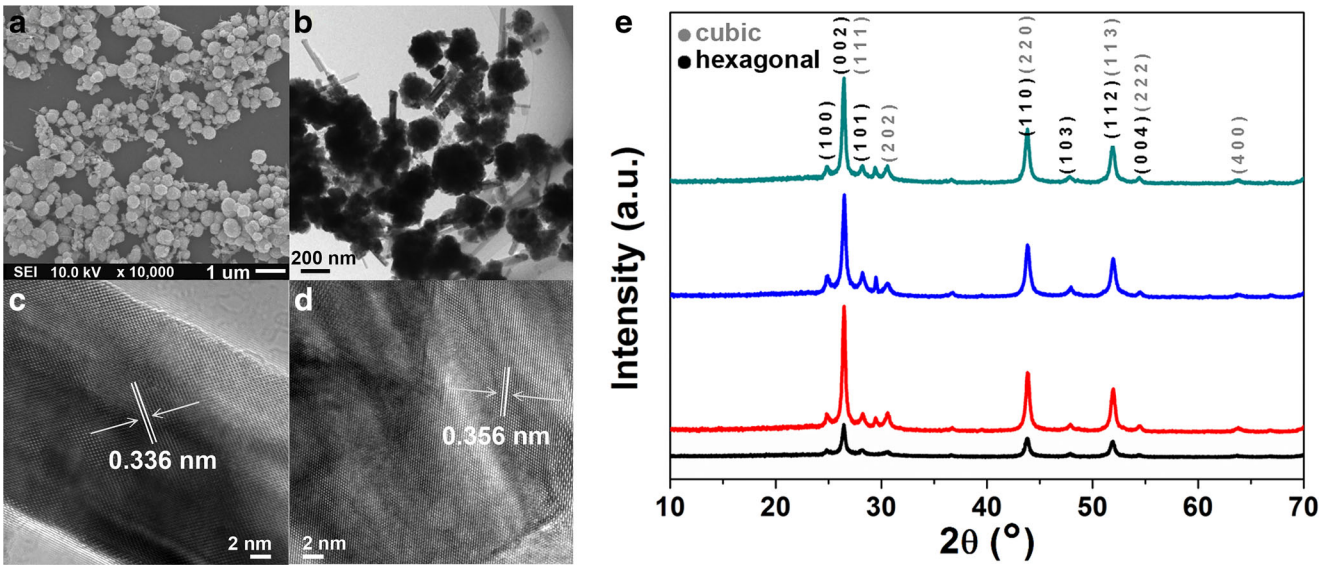

Fig. 2 Typical SEM (**a**), TEM (**b**), HRTEM (**c**, **d**) images of mp–CdS@BC–2; and (**e**) PXRD patterns of mp–CdS (black) and mp–CdS@BC–n (n = 1, red; 2, blue; and 3, grayish green)

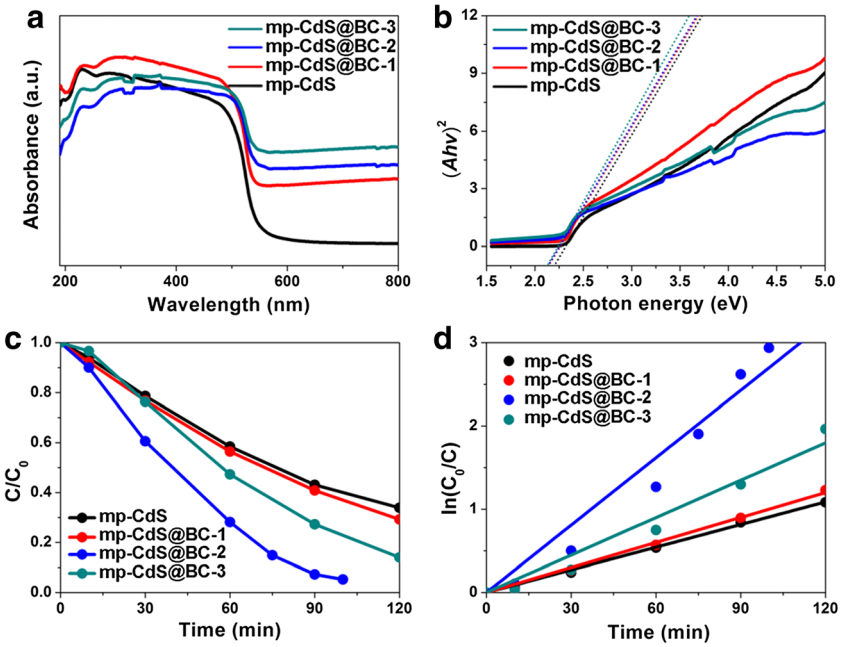

Fig. 3 UV–vis DRS spectra (**a**), K–M plots (**b**), RhB degradation efficiency (**c**), and plot of ln (C_0/C) as a function of irradiation time for mp–CdS and mp–CdS@BC–n (n = 1, 2, and 3) (**d**)

contribute to the overall visible light–driven catalytic processes, as indicated by the elemental analyses (Table 1). In order to quantify the reaction kinetics of RhB degradation in this current work, the pseudo-first-order model was employed to calculate rate constant (κ) of the photocatalytic reactions (Fig. 3d) (Ning et al. 2016; Li et al. 2006). The mp–CdS@BC–2 showed the highest photocatalytic efficiency ($\kappa = 2.7 \times 10^{-2}$ min^{-1}) which was approximately 3-fold that of the mp–CdS ($\kappa = 9.1 \times 10^{-3}$ min^{-1}). These results indicated that BCs might play a vital role for the enhanced RhB degradation efficiency (Huang et al. 2018).

Stability and reusability

In general, stability and reusability of the photocatalysts are key factors deciding their practical applications. For this purpose, cycling reactions of RhB degradation were performed to verify the photostability and reusability of mp–CdS@BC–2. It was investigated that the mp–CdS@BC–2 composite photocatalyst could retain more than 80% of the initial photocatalytic ability at the end of four consecutive runs, as shown in Fig. 4a. The decrease of catalytic efficiency might be caused by particle the aggregation and deactivation of CdS (Fig. S4; ESI), and possible insignificant loss of photocatalysts during the recover processes. PXRD patterns were recorded after cycling reactions and the recycled mp–CdS@BC–2 displayed identical characteristics to those identified for the as-prepared sample (Fig. 4b). These results confirmed the structural and crystalline stability of composite photocatalysts upon the introduction of BC supports that may greatly favor the stabilization of mp–CdS NPs.

Probable reacting mechanism

Radicals generated during photocatalysis, such as h^+, •OH and O_2•$^-$, can play distinguishable roles for the degradation of organic pollutants (Wang et al. 2014). Therefore, the degradation efficiency was tested to recognize the effects of different radicals using various scavengers. Significant decreases on the photocatalytic efficiency of

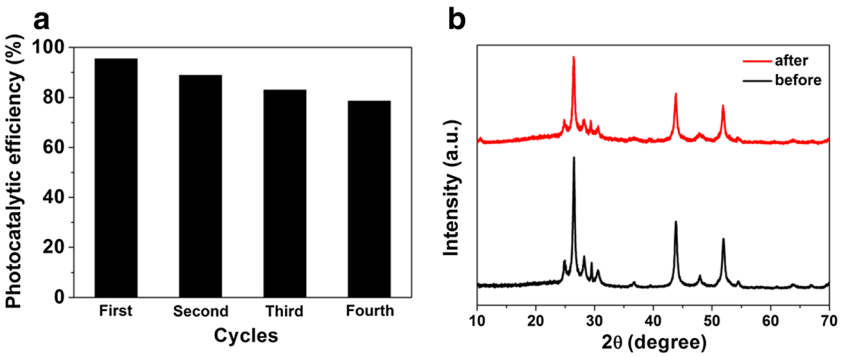

Fig. 4 (**a**) Photocatalytic efficiency of mp–CdS@BC–2 in recycling reaction of RhB degradation and (**b**) PXRD of as-prepared and recycled mp–CdS@BC–2 samples

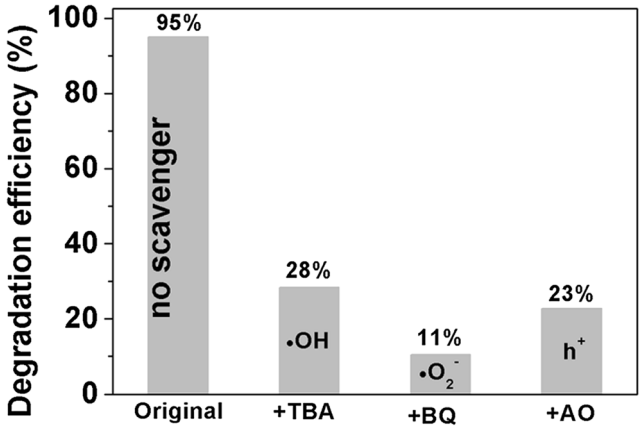

Fig. 5 Degradation efficiency of mp–CdS@BC–2 with exposure to various scavengers

mp–CdS@BC–2 were discovered upon addition of tert–butyl alcohol (TBA), benzoquione (BQ), and ammonium oxalate (AO), which are typical scavengers for •OH, O_2•$^-$, and h^+ radicals, respectively (Meng et al. 2011). Specifically, BQ exhibited the strongest quenching effects toward photocatalytic reactions, which was considerably superior to AO and TBA. These results suggested O_2•$^-$ radicals were likely dominant active species, whereas h^+ and •OH radicals played relatively minor roles (Fig. 5).

Visible light–driven photocatalysis in this system might be initiated by the fast generation and separation of photogenerated carriers (h^+, e^-), rationalized by electron transfer from the VB to CB of CdS (Bera et al. 2015). The highly reductive e^- takes part in the formation of a series of active species including •OH and O_2•$^-$ radicals, of which OH• is initiated via a complex process involving the reduction of H_2O_2 generated by O_2•$^-$ species. The oxidative h^+, •OH and O_2•$^-$ attack organic substrates and degrade RhB into secondary and final products (H_2O and CO_2). Meanwhile, the presence of microporous BC supports effectively increases the accumulation of RhB molecules on surfaces of the composite photocatalysts. The accumulated RhB are consequently photodegraded via accepting active species from the composite photocatalysts.

Conclusion

In summary, a series of composite photocatalysts have been prepared through the deposition of mixed phase CdS (mp–CdS) nanoparticles (NPs) on surfaces of activated biomass carbons (BCs). The mp–CdS@BC composite photocatalysts have been applied for efficient RhB degradation under visible irradiation. The composite photocatalysts have displayed reduced band gap energy and considerable specific surface area, which are superior for their excellent light adsorption ability and RhB accumulation. The photocatalytic degradation of RhB has been evaluated and the mp–CdS@BC–2 exhibits the highest degradation efficiency which was about 3-fold that of the mp–CdS precursor. Moreover, the mp–CdS@BC–2 also demonstrates excellent catalytic stability in cyclic experiments. This study provides a facile and effective pathway for the preparation of viable visible light–driven photocatalysts. Future study focusing on the size effect of mp–CdS NPs is currently underway.

Funding information This work received financial support from the International Science and Technology Cooperation and Exchange Project of Fujian Agriculture and Forestry University (Grant KXGH17010), the State Key Laboratory of Structural Chemistry (Grant 20170032), and the New Century Excellent Talents in Fujian Province University, Fujian Agriculture and Forestry University Program for Distinguished Young Scholar (Grant xjq201813).

References

Apte SK, Garaje SN, Valant M, Kale BB (2012) Eco–friendly solar light driven hydrogen production from copious waste H_2S and organic dye degradation by stable and efficient orthorhombic CdS quantum dots–GeO_2 glass photocatalyst. Green Chem 14(5):1455–1462

Aricò AS, Bruce P, Scrosati B, Tarascon JM, Schalkwijk WV (2005) Nanostructured materials for advanced energy conversion and storage devices. Nat Mater 4:366–377

Bera R, Kundu S, Patra A (2015) 2D hybrid nanostructure of reduced graphene oxide–CdS nanosheet for enhanced photocatalysis. ACS Appl Mater Interfaces 7(24):13251–13259

Bunmahotama W, Hung WN, Lin TF (2017) Prediction of the adsorption capacities for four typical organic pollutants on activated carbons in natural waters. Water Res 111:28–40

Chen X, Shen S, Guo L, Mao SS (2010) Semiconductor–based photocatalytic hydrogen generation. Chem Rev 110(11):6503–6570

Dai L, Chang DW, Baek JB, Lu W (2012) Carbon nanomaterials for advanced energy conversion and storage. Small 8(8):1130–1166

Dai X, Xie M, Meng S, Fu X, Chen S (2014) Coupled systems for selective oxidation of aromatic alcohols to aldehydes and reduction of nitrobenzene into aniline using CdS/g–C_3N_4 photocatalyst under visible light irradiation. Appl Catal B Environ 158:382–390

Fang G, Liu C, Wang Y, Dionysiou DD, Zhou D (2017) Photogeneration of reactive oxygen species from biochar suspension for diethyl phthalate degradation. Appl Catal B Environ 214:34–45

Han TYJ, Worsley MA, Baumann TF, Satcher JH Jr (2011) Synthesis of ZnO coated activated carbon aerogel by simple sol–gel route. J Mater Chem 21(2):330–333

Harvey OR, Kuo LJ, Zimmerman AR, Louchouarn P, Amonette JE, Herbert BE (2012) An index–based approach to assessing recalcitrance and soil carbon sequestration potential of engineered black carbons (biochars). Environ Sci Technol 46(3):1415–1421

Huang HB, Wang Y, Jiao WB, Cai FY, Shen M, Zhou SG, Cao HL, Lü J, Cao R (2018) Lotus–leaf–derived activated–carbon–supported nano–CdS as energy–efficient photocatalysts under visible irradiation. ACS Sustain Chem Eng 6:7871–7879

Huggins TM, Haeger A, Biffinger JC, Ren ZJ (2016) Granular biochar compared with activated carbon for wastewater treatment and resource recovery. Water Res 94:225–232

Jang JS, Yu CJ, Choi SH, Ji SM, Kim ES, Lee JS (2008) Topotactic synthesis of mesoporous ZnS and ZnO nanoplates and their photocatalytic activity. J Catal 254(1):144–155

Jing F, Liang R, Xiong J, Chen R, Zhang S, Li Y, Wu L (2017) MIL–68(Fe) as an efficient visible–light–driven photocatalyst for the treatment of a simulated waste–water contain Cr(VI) and Malachite Green. Appl Catal B Environ 206(5):9–15

Li Y, Li X, Li J, Yin J (2006) Photocatalytic degradation of methyl orange by TiO_2–coated activated carbon and kinetic study. Water Res 40(6): 1119–1126

Li K, Chen R, Li SL, Han M, Xie SL, Bao JC, Dai ZH, Lan YQ (2015) Self–assembly of a mesoporous ZnS/mediating interface/CdS heterostructure with enhanced visible–light hydrogen–production activity and excellent stability. Chem Sci 6:5263–5268

Li K, Han M, Chen R, Li SL, Xie SL, Mao C, Bu X, Cao XL, Dong LZ, Feng P, L YQ (2016) Hexagonal@cubic CdS core@shell nanorod photocatalyst for highly active production of H_2 with unprecedented stability. Adv Mater 28(40):8906–8911

Liu S, Li C, Yu J, Xiang Q (2011) Improved visible–light photocatalytic activity of porous carbon self–doped ZnO nanosheet-assembled flowers. CrystEngComm 13(7):2533–2541

Matos J, Laine J, Herrmann JM (2001) Effect of the type of activated carbons on the photocatalytic degradation of aqueous organic pollutants by UV–irradiated titania. J Catal 200(1):10–20

Meng S, Li D, Sun M, Li W, Wang J, Chen J, Fu X, Xiao G (2011) Sonochemical synthesis, characterization and photocatalytic properties of a novel cube-shaped $CaSn(OH)_6$. Catal Commun 12(11): 972–975

Ning X, Meng S, Fu X, Ye X, Chen S (2016) Efficient utilization of photogenerated electrons and holes for photocatalytic selective organic syntheses in one reaction system using a narrow band gap CdS photocatalyst. Green Chem 18(12):3628–3639

Panneri S, Ganguly P, Mohan M, Nair BN, Mohamed PAA, Warrier KG, Hareesh US (2017) Photoregenerable, bifunctional granules of carbon–doped g–C_3N_4 as adsorptive photocatalyst for the efficient removal of tetracycline antibiotic. ACS Sustain Chem Eng 5(2): 1610–1618

Poizot P, Dolhem F (2011) Clean energy new deal for a sustainable world: from non–CO_2 generating energy sources to greener electrochemical storage devices. Energy Environ Sci 4(6):2003–2019

Rawal A, Joseph SD, Hook JM, Chia CH, Munroe PR, Donne S, Lin Y, Phelan D, Mitchell DRG, Pace B, Horvat J, Webber JBW (2016) Mineral–biochar composites: molecular structure and porosity. Environ Sci Technol 50(14):7706–7714

Singh BP, Cowie AL, Smernik RJ (2012) Biochar carbon stability in a clayey soil as a function of feedstock and pyrolysis temperature. Environ Sci Technol 46(21):11770–11778

Su H, Fang Z, Tsang PE, Fang J, Zhao D (2016) Stabilisation of nanoscale zero–valent iron with biochar for enhanced transport and in–situ remediation of hexavalent chromium in soil. Environ Pollut 214:94–100

Wang P, Xian J, Chen J, He Y, Wang J, Li W, Shao Y, Li D (2014) Preparation, photocatalytic activity, and mechanism of $Cd_2Sb_2O_{6.8}$–graphene composite. Appl Catal B Environ 144:644–653

Woolf D, Amonette JE, Street-Perrott FA, Lehmann J, Joseph S (2010) Sustainable biochar to mitigate global climate change. Nat Commun 1. https://doi.org/10.1038/ncomms1053.

Wu X, Zhao J, Wang L, Han M, Zhang M, Wang H, Huang H, Liu Y, Kang Z (2017) Carbon dots as solid–state electron mediator for $BiVO_4$/CDs/CdS Z–scheme photocatalyst working under visible light. Appl Catal B Environ 206(5):501–509

Xiang Q, Yu J, Jaroniec M (2012) Synergetic effect of MoS2 and graphene as cocatalysts for enhanced photocatalytic H2 production activity of TiO2 nanoparticles. J Am Chem Soc 134(15):6575–6578

Xue X, Zang W, Deng P, Wang Q, Xing L, Zhang Y, Wang ZL (2015) Piezo–potential enhanced photocatalytic degradation of organic dye using ZnO nanowires. Nano Energy 13:414–422

Zhang X, Zhou M, Lei L (2005) Preparation of photocatalytic TiO_2 coatings of nanosized particles on activated carbon by AP–MOCVD. Carbon 43(8):1700–1708

Zhao Y, Zhang X, Zhai J, Jiang L, Liu Z, Nishimoto S, Murakami T, Fujishima A, Zhu D (2008) Ultrastable TiO_2 foams derived macro–/meso–porous material and its photocatalytic activity. Microporous Mesoporous Mater 116(1–3):710–714